Journal of Thermal Analysis and Calorimetry, Vol. 80 (2005) 613–618

THERMOANALYTICAL INVESTIGATION OF TIN AND CERIUM SALT MIXTURES

Ana Brăileanu[1*], *Susana Mihaiu*[1], *Margit Bán*[2], *J. Madarász*[2] *and G. Pokol*[2]

[1]Institute of Physical Chemistry, 202 Spl. Independenþei, 060021 Bucharest, Roumania
[2]Institute of General and Analytical Chemistry, Budapest University of Technology and Economics, Szt. Gellért tér 4, 1521 Budapest, Hungary

Oxide materials belonging to the Sn–Ce–O system are very interesting due to their use as solid electrolytes in fuel cells, catalysts, sensors and photoanodes in solar cells.

The aim of the present work is to investigate the thermal behaviour of some tin and cerium salt mixtures. Mixtures with different representative Sn:Ce atomic ratio were prepared by classical ceramic method using SnC_2O_4, $Ce(SO_4)_2\cdot 4H_2O$ and $(NH_4)_2Ce(NO_3)_6$ as starting compounds. The samples were investigated by means of TG/DTA methods in flowing and static air atmosphere. SnO_2 and/or CeO_2 were identified by X-ray diffraction and IR spectroscopy in the final decomposition products, depending on the initial composition of the both series. A different crystallinity degree of the solid products was observed depending on the Ce precursor.

Keywords: *IR spectroscopy, thermal behaviour, tin and cerium salt mixtures, X-ray diffraction*

Introduction

Oxide materials with pre-established properties can be obtained by different synthesis routes using suitable precursors. Thermal decomposition of some selected tin and cerium precursors was used for the obtaining of the Sn–Ce–O materials. These materials are of practical interest due to their use in a wide variety of applications. Sensors obtained by doping SnO_2 with CeO_2 present good sensitivity, high selectivity and quick response to CH_4 and H_2S even at room temperature [1, 2]. The redox properties of $Sn_{1-x}Ce_xO_2$ mixed oxides allowed their use as high-activity catalysts [3–5]. The compositions with CeO_2 content>80 mol% belonging to the SnO_2–CeO_2 binary system attracted interest for obtaining electrochromic layers exhibiting large optical transmission variation in UV, VIS and IR range [6]. Mixed CeO_2/SnO_2 film electrodes were used as photoanodes in a new generation of nanophase solar cells [7]. Tin dioxide-doped ceria materials are potential electrolytes for solid oxide fuel cells (SOFC) [8].

Tin dioxide solids with experimental density close to the theoretical one have been prepared from nanometric powders resulted from tin(II) oxalate thermal decomposition [9]. According to literature data, tin(II) oxalate is mentioned as being one of the few precursors for SnO preparation, usually unstable, which turns into SnO_2 [10]. The experimental conditions of the tin(II) oxalate controlled decomposition (atmosphere, thermal history, different additives) lead to the formation of expected defects in the rutile-type SnO_2 structure [11].

Cerium salts were selected taking into account the temperature of their complete decomposition. Thus, $(NH_4)_2Ce(NO_3)_6$ decomposes in the same temperature range as tin(II) oxalate and $Ce(SO_4)_2\cdot 4H_2O$ has its final decomposition step in the range where the SnO_2 lattice becomes less stable [12]. The decomposition mechanism of both cerium precursors has not been elucidated and literature data are partly contradictory regarding the oxidation state of the cerium ion during the thermal treatment, but all authors agree with CeO_2 as final product.

The present study deals with the mutual influence of the cerium inorganic salts and tin(II) oxalate decomposition in order to obtain materials with pre-established properties.

Experimental

Sample preparation

The raw materials were p.a. grade tin(II) oxalate (Fluka), cerium(IV) sulfate tetrahydrate (Fluka) and cerium(IV) ammonium nitrate (Loba Feinchemie).

The studied mixtures have been prepared by dry homogenization of SnC_2O_4, $Ce(SO_4)_2\cdot 4H_2O$ and $(NH_4)_2Ce(NO_3)_6$ compounds. Table 1 presents the composition of the studied samples.

---

[*] Author for correspondence: abrail@chimfiz.icf.ro

1388–6150/$20.00

Akadémiai Kiadó, Budapest, Hungary
Springer, Dordrecht, The Netherlands

Table 1 Composition of the studied mixtures

No.	Sample	Starting compounds	Sn:Ce atomic ratio
1	1-OS	SnC_2O_4+$Ce(SO_4)_2 \cdot 4H_2O$	39:1
2	1-ON	SnC_2O_4+$(NH_4)_2Ce(NO_3)_6$	39:1
3	2-OS	SnC_2O_4+$Ce(SO_4)_2 \cdot 4H_2O$	1:1
4	2-ON	SnC_2O_4+$(NH_4)_2Ce(NO_3)_6$	1:1
5	3-OS	SnC_2O_4+$Ce(SO_4)_2 \cdot 4H_2O$	1:4
6	3-ON	SnC_2O_4+$(NH_4)_2Ce(NO_3)_6$	1:4

Sample characterization

The thermal behaviour of the precursors and of the mixtures was studied up to 500°C using a STD 2960 simultaneous DTA and TG/DTG apparatus (TA Instruments); heating rate: 10 K min^{-1}; flowing air atmosphere: 10 L min^{-1} and helium atmosphere. In addition, TG-DTA investigations were performed up to 1000ºC, in static air atmosphere with α-Al_2O_3 as reference material with a heating rate of 5 K min^{-1}. A Paulik–Paulik–Erdey Derivatograph (model OD-103, MOM, Hungary) was used.

X-ray diffractograms were recorded for the samples resulting from non-isothermal treatments with a HZG-4 (FPM-Zeiss) diffractometer using CuK_α radiation (λ=1.54056) with Ni filter.

IR spectra were recorded in the 4000–200 cm^{-1} range with a Carl Zeiss Jena Specord 80 Spectrophotometer.

Results and discussion

Precursors

Some results of the thermal decomposition study of cerium(IV) ammonium nitrate in flowing air and N_2 were reported in [13] and thermal behaviour of tin(II) oxalate, cerium(IV) ammonium nitrate and cerium(IV) sulfate tetrahydrate in static air was presented in [14].

DTA and TG curves of the three precursors recorded in static air up to 1000ºC are presented in Fig. 1, in order to evidence the thermal behaviour of the mixtures in comparison to that of the precursors.

The final decomposition product of tin(II) oxalate is SnO_2.

The decomposition of cerium(IV) sulfate tetrahydrate shows several decomposition steps (Fig. 1, curve 2): the loss of water, with the subsequent formation of an intermediate compound, probably $3CeO_2 \cdot 4SO_3$ or $Ce_2(SO_4)_3$, followed by the thermal evolution of sulphur oxides. The final decomposition product is CeO_2.

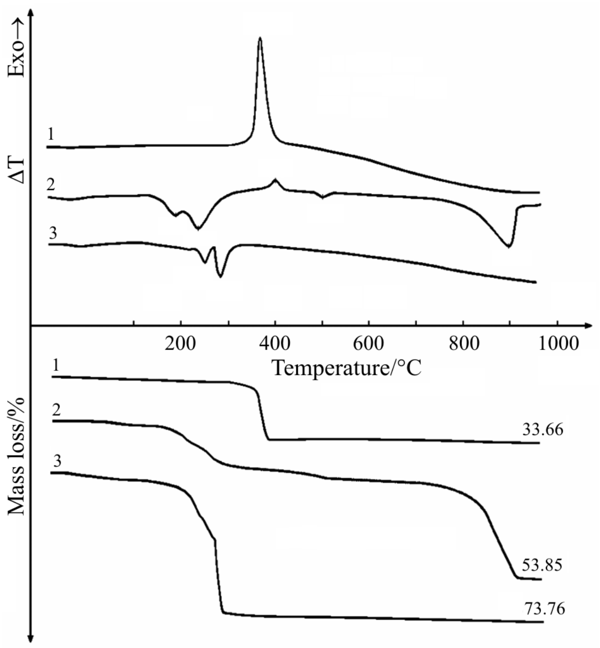

Fig. 1 DTA/TG curves of the precursors recorded in static air up to 1000°C: 1 – SnC_2O_4, 2 – $Ce(SO_4)_2 \cdot 4H_2O$, 3 – $(NH_4)_2Ce(NO_3)_6$

Commercial $(NH_4)_2Ce(NO_3)_6$ decomposes up to 300ºC with large overlapping of the successive steps (Fig. 1, curve 3). CeO_2 is also the final decomposition product.

Mixtures

Thermal analysis in flowing air

Simultaneous DTA/TG curves of the mixtures studied, up to 500ºC, are shown in Figs 2a, b and c.

The curves of samples 1-ON and 1-OS (Fig. 2a) are similar and present an exothermic effect in the same temperature range as tin(II) oxalate, as was expected, because the contribution of the cerium precursors in the average molecular mass is small. For the mixture 1-ON one can observe a broadening of the decomposition range compared to the mixture 1-OS.

For samples 2-ON and 2-OS (Fig. 2b) the curves show significant differences. Thus, the thermal behavior of the mixture 2-OS exhibits the thermal effects of both precursors, water evolution from $Ce(SO_4)_2 \cdot 4H_2O$ and SnC_2O_4 combustion. For the mixture 2-ON, a low temperature endothermic effect due to the adsorbed water and an overlapping of the endothermic decomposition effects of cerium nitrate with tin oxalate combustion effect (shifted with more than 100ºC to lower temperatures), can be noticed.

The thermal behaviour of sample 3-OS (Fig. 2c) pointed out the broadening of the water evolution range (comparatively with $Ce(SO_4)_2 \cdot 4H_2O$), with more distinct effects and the lack of the SnC_2O_4 com-

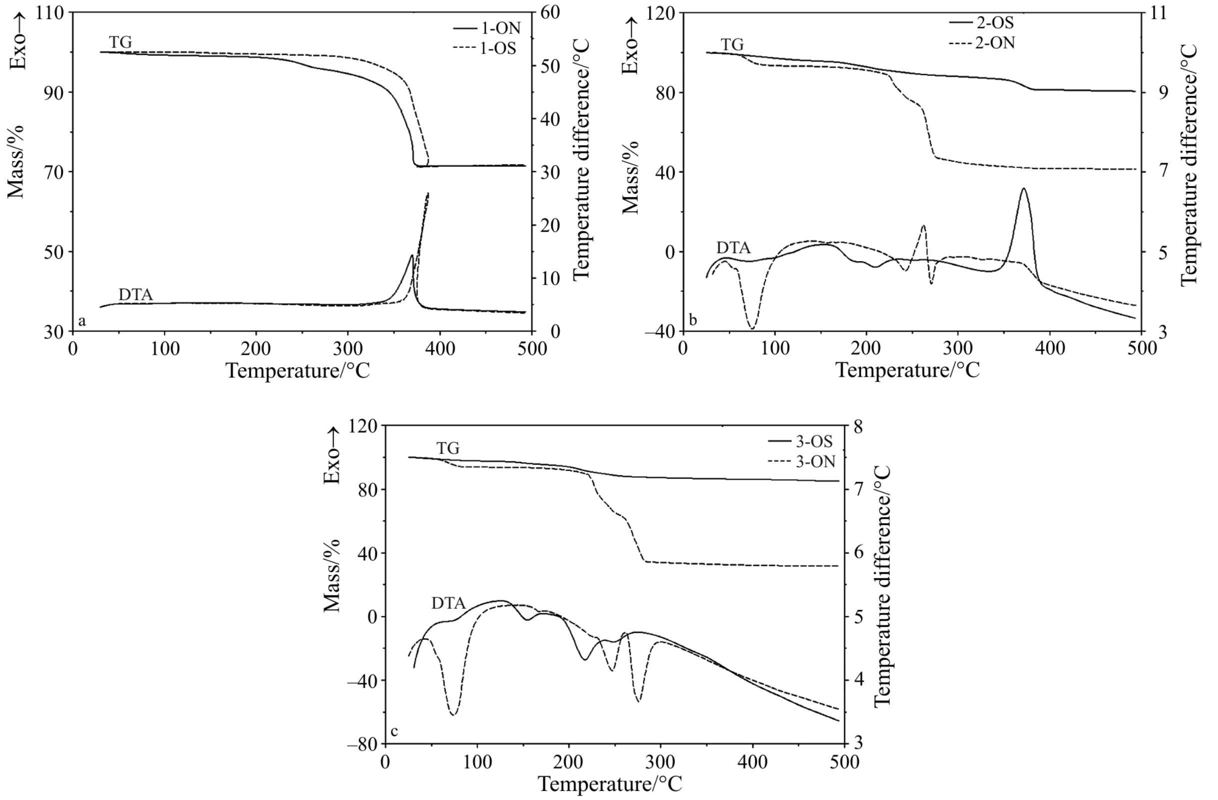

Fig. 2 TG/DTA curves of the mixtures studied, up to 500ºC, in flowing air: a – 1-ON and 1-OS, b – 2-ON and 2-OS, c – 3-ON and 3-OS

bustion effect. Sample 3-ON gave DTA/TG curves quite similar to sample 2-ON.

Table 2 summarizes the mass changes of the samples thermally treated up to 500ºC, in flowing air and the identified phases by X-ray diffraction in the residues.

X-ray diffraction patterns for samples 1-OS and 1-ON are similar to pure tin(II) oxalate residue in air at 500ºC as it was expected. Broad peaks of SnO_2 and low intensity first peak of SnO are present. In the residue of the sample 2-OS only low crystallinity SnO_2 was identified (SnC_2O_4 decomposition is complete up to 400ºC). No information regarding intermediate decomposition products of $Ce(SO_4)_2{\cdot}4H_2O$ was supplied by X-ray diffraction. The possible intermediate decomposition products of the $Ce(SO_4)_2{\cdot}4H_2O$, taking into account the literature data, are the following: $Ce(SO_4)_2$, $Ce_2(SO_4)_3$ and $3CeO_2{\cdot}4SO_3$. The best agreement between experimental and calculated residues indicates that $Ce(SO_4)_2$ is the most probable intermediate compound. The same compound could hinder the SnO_2 lattice formation in the case of the sample 3-OS. Only very broad peaks of CeO_2 (JCPDS 43-1002) with low intensities are detected in the final decomposition products of the samples 2-ON and 3-ON. The lack of the characteristic SnO_2 peaks could be due to the formation of nanometer order size SnO_2 particles [15].

Thermal analysis in static air

DTA curves of the studied samples presented in Figs 3a, b and c were measured up to 1000ºC with a heating rate of 5 K min^{-1}.

Table 2 Characteristics of the samples thermally treated up to 500ºC in flowing air

No.	Sample	Experimental residue/ mass%	Possible compounds in the residue/ mol%	Theoretical residue/ mass%	Identified phases in the residue
1	1-OS	71.19	$97.5SnO_2+2.5Ce(SO_4)_2$	73.25	SnO_2+SnO
2	1-ON	71.41	$97.5SnO_2+2.5CeO_2$	70.26	SnO_2+SnO
3	2-OS	80.63	$50SnO_2+50Ce(SO_4)_2$	79.11	SnO_2 (l.c.)*
4	2-ON	41.50	$50SnO_2+50CeO_2$	42.74	CeO_2 (l.c.)*
5	3-OS	85.03	$20SnO_2+80Ce(SO_4)_2$	83.67	amorphous
6	3-ON	31.67	$20SnO_2+80CeO_2$	34.98	CeO_2 (l.c.)*

(l.c.)* – low crystallinity

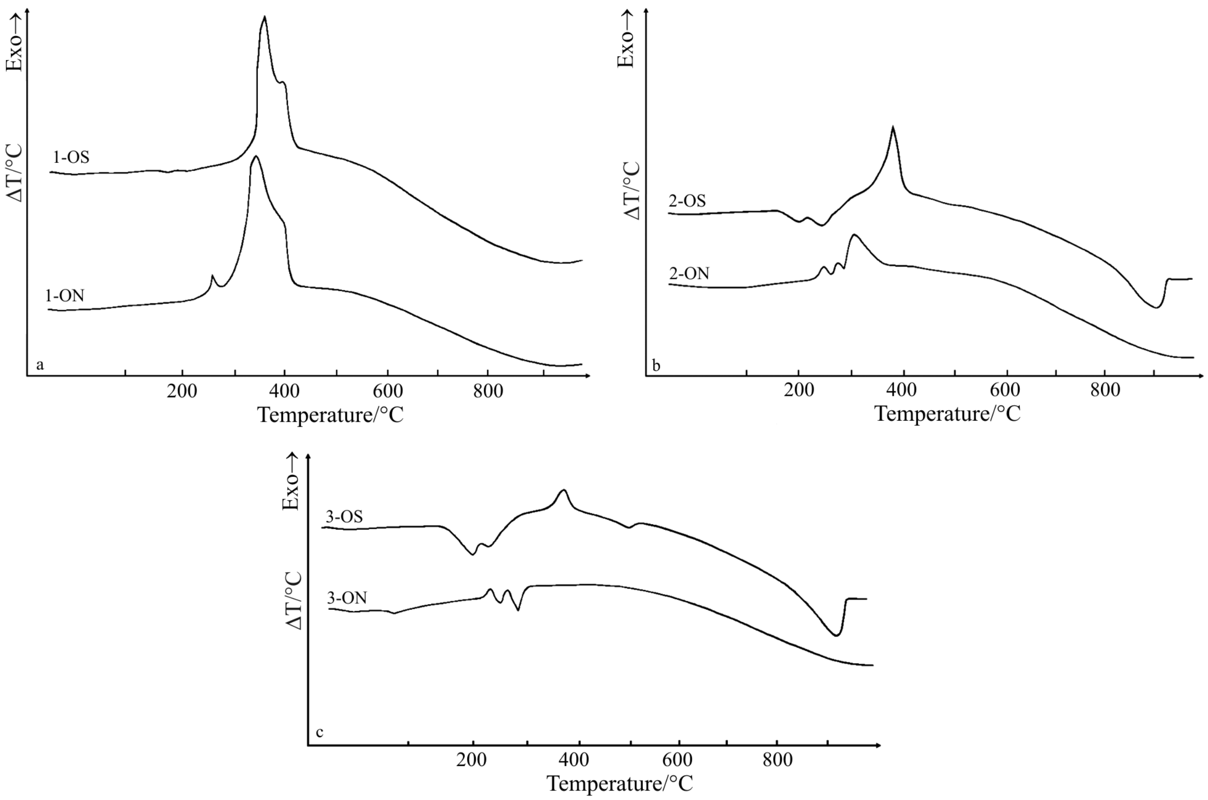

Fig. 3 DTA curves of the studied samples up to 1000ºC, in static air: a – 1-ON and 1-OS, b – 2-ON and 2-OS, c – 3-ON and 3-OS

Some differences are noticed in comparison with the DTA/TG curves previously presented. Both DTA curves for mixtures 1-ON and 1-OS (Fig. 3a) show one shoulder on the exothermic SnC_2O_4 combustion effect. The presence of cerium precursors in the mixtures as well as different heating conditions (in static air 5 and in flowing air 10 K min^{-1}) could be the reason why Sn oxalate combustion and $Sn^{2+} \rightarrow Sn^{4+}$ oxidation are not simultaneous compared to pure Sn oxalate. DTA curves for the samples 2-ON and 3-ON analyzed in static air prior to the measurements in flowing air do not show highly endothermic effects below 100ºC. Probably the storing conditions of the powders led to the presence of the above mentioned effects on DTA curves obtained in flowing air.

The thermal behavior of mixture 2-OS exhibits, as in flowing air atmosphere, the thermal effects of both precursors, SnC_2O_4 and $Ce(SO_4)_2 \cdot 4H_2O$, with maxima in distinct temperature ranges. Mutual influence of the cerium ammonium nitrate decomposition and tin(II) oxalate combustion, shifted with ~80ºC to lower temperatures, can also be emphasized for the sample 2-ON (Fig. 3b).

The DTA curve of mixture 3-OS (Fig. 3c) is quite similar to that of sample 2-OS, with a less pregnant SnC_2O_4 combustion effect (according to the ratio of the precursors) but visible, unlike in flowing air conditions. The endothermic high temperature effect due to the final decomposition process is shifted to lower temperatures both for the samples 2-OS and the 3-OS. Similar thermal behaviour, both in flowing and static air, was observed in the case of sample 3-ON.

The experimental and calculated residues (mass%) of the studied samples thermally treated up to 1000ºC are presented in Table 3.

The calculated residue was obtained with the assumption of mixtures of SnO_2 and CeO_2 with respect to the initial Sn:Ce atomic ratio. A good agreement between experimental and calculated values can be pointed out.

X-ray patterns of the DTA/TG residues are presented in Fig. 4.

X-ray diffraction patterns of the non-isothermally treated samples show that different phases were formed, according to the initial Sn:Ce atomic ratio.

X-ray data indicate, for the products of samples 1-ON and 1-OS, the presence of the SnO_2 (JCPDS 21-1250) with a rutile-type structure and possible SnO traces.

For samples 2-ON and 2-OS one can notice the presence of both rutile- and fluorite-type phases. Only one phase, CeO_2 (JCPDS 75-0390) with a fluorite-type structure, was identified in the products of samples 3-ON and 3-OS.

Although the final decomposition temperature of $Ce(SO_4)_2 \cdot 4H_2O$ is ~920ºC (close to the final anneal-

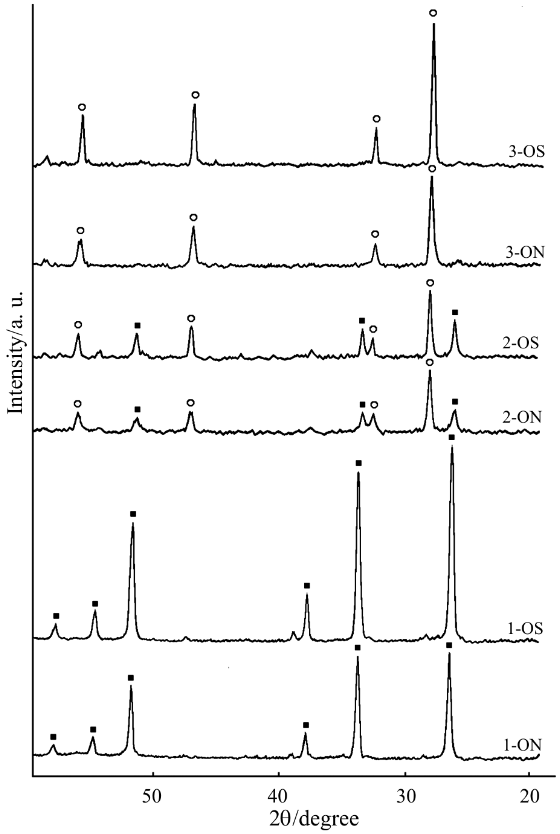

Fig. 4 X-ray diffraction patterns of the DTA/TG residues, at 1000ºC; ■ – SnO_2, ○ – CeO_2

ing temperature of the mixtures), the CeO_2 lattice is better developed in the residues of the OS series, compared to the ON series.

Supplementary information about the changes in the structure of the samples obtained by the thermal decomposition was supplied in evidence by IR spectroscopy. IR spectra for precursors, initial mixtures and non-isothermally treated samples up to 1000ºC were measured. IR spectrum for $Ce(SO_4)_2 \cdot 4H_2O$ is similar to that published in [16]. The characteristic absorption bands of SnC_2O_4 and $(NH_4)_2Ce(NO_3)_6$ were assigned taking into account the literature IR spectra of the same type compounds. IR spectra for initial mixtures show the characteristic bands of the starting components as: oxalate (1620, 1370–1290 cm^{-1}), sulfate (1189–1100, 600 cm^{-1}), molecular water (1600 cm^{-1}), NH group (3300–3000 cm^{-1}), NH_4^+ (1550, 1400 cm^{-1}) and NO_3^- (1460, 1300–700 cm^{-1}). For non-isothermally treated samples, the vanishing of the above mentioned characteristic bands could be observed. IR spectra of the studied samples, in the 1600–200 cm^{-1} range, are presented in Figs 5a, b and c).

The IR spectra of samples 1-OS and 1-ON, non-isothermally treated up to 1000ºC, show the characteristic bands of SnO_2 lattice. The shoulder at about 500^{-1}, in the case of sample 1-OS, can be assigned to CeO_2. The samples 2-OS and 2-ON show the characteristic bands of SnO_2 (700–600 cm^{-1}) and CeO_2 (500–300 cm^{-1}) [17]. One can notice, for the sample

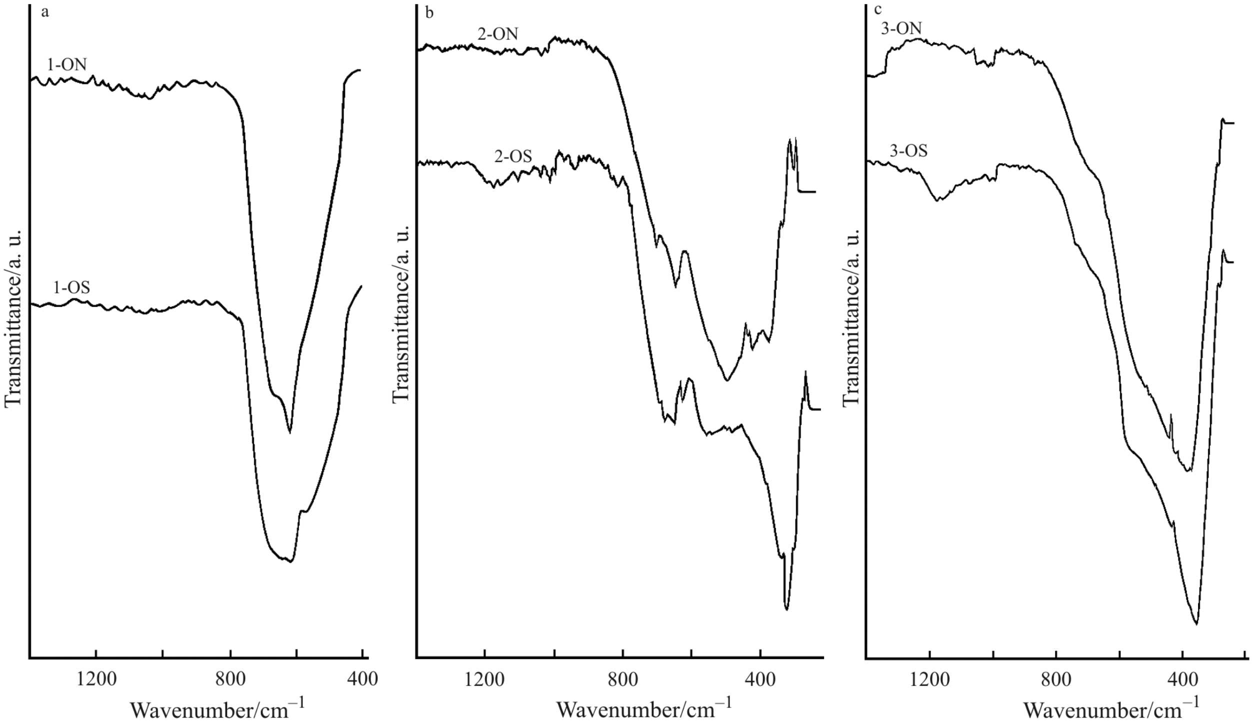

Fig. 5 IR spectra of the studied samples, non-isothermally treated up to 1000ºC: a – 1-ON and 1-OS, b – 2-ON and 2-OS, c – 3-ON and 3-OS

Table 3 Characteristics of the samples thermally treated up to 1000ºC, in static air at 5 K min^{-1}

No.	Sample	Residue/mass%		Phases identified by X-ray diffraction
		exp.	calc.	
1	1-OS	68.21	71.45	SnO_2
2	1-ON	68.26	70.26	SnO_2
3	2-OS	54.50	52.83	SnO_2+CeO_2
4	2-ON	39.41	42.76	SnO_2+CeO_2
5	3-OS	46.86	47.47	CeO_2
6	3-ON	31.01	34.88	CeO_2

2-OS, the presence of the characteristic bands assigned to the Sn–O bond situated at 320 cm^{-1}. Only a broad CeO_2 characteristic band, situated between 800 and 300 cm^{-1} can be observed for the samples 3-OS and 3-ON. IR results confirm X-ray data.

Conclusions

Mixtures of tin(II) oxalate with $Ce(SO_4)_2 \cdot 4H_2O$ (OS series) and with $(NH_4)_2Ce(NO_3)_6$ (ON series), in representative different Sn:Ce atomic ratios, were investigated by thermal analysis in flowing and static air.

DTA and TG/DTG data pointed out that, for the ON series, thermal decomposition is complete by ~400ºC, while for the OS series, by ~950ºC. DTA curves for the ON series indicated an overlapping of the $(NH_4)_2Ce(NO_3)_6$ decomposition with SnC_2O_4 combustion effects. For OS series, the thermal effects of both precursors with maxima in distinct temperature range were observed. $Ce(SO_4)_2$ is a possible intermediate in the thermal decomposition up to 500ºC of the OS series according to the mass changes. Further investigations are required to clarify the thermal decomposition mechanism.

Rutile-type phase (SnO_2) and/or fluorite-type phase (CeO_2) were identified by X-ray diffraction and IR spectroscopy in the final decomposition products, depending on the initial composition of the mixtures of both series.

Residues of the ON series with a lower degree of crystallinity suggest these materials may be used as high-activity catalysts. Preferential ordering of the cubic fluorite structure established in samples with Sn:Ce atomic ratio ≤1 belonging to both series can be of interest in preparing solid electrolytes for SOFC.

References

1 G. Fang, Z. Liu, C. Liu and K. Yao, Sens. Actuators, B66 (2000) 46.
2 N. Butta, L. Cinquengrani, E. Mugno, A. Tagliente and S. Pizzini, Sens. Actuators, B6 (1992) 253.
3 R. Sasikala, N. M. Gupta and S. C. Kulschreshtha, Catal. Lett., 71 (2001) 69.
4 R. Lin, Y. J. Zhong, M. F. Luo and W. P. Liu, Indian J. Chem., Sect. A, 40 (2001) 36.
5 T. M. Jyothi, M. B. Talawar and B. S. Rao, Catal. Lett., 64 (2000) 151.
6 M. A. Aegerter, C. B. Avvelaneda, A. Pawlica and M. Atik, J. Sol-Gel Sci. Technol., 8 (1997) 689.
7 A. Turković and Z. Crnjak Orel, Sol. Energy Mater. Sol. Cells, 45 (1997) 275.
8 M. Feng and J. B. Goodenough, Eur. J. Solid State Inorg. Chem., T31 (1994) 663.
9 K. Uematsu, ‘Sintering of Advanced Materials-Applications of hot isostatic pressing’, Ed. by K. Tanaka and K. Ishizuka, Uchida Rokakuho, Tokyo, Japan 1987, p. 77.
10 C. Macarovici, ‘Inorganic Chemistry’ (in Roumanian) Ed. Didactică şi Pedagogică, Bucureşti 1972, p. 251.
11 S. Mihaiu, O. Scarlat, Gh. Aldica and M. Zaharescu, J. Eur. Ceram. Soc., 21 (2001) 1801.
12 J. Maier and W. J. Goepel, Solid State Chem., 72 (1988) 293.
13 G. Pokol, T. Leskelä and L. Niinistö, J. Thermal Anal., 42 (1994) 343.
14 S. Mihaiu, A. Brăileanu, D. Crişan and M. Zaharescu, Rev. Roum. Chim., 48 (2003) 939.
15 S. Mihaiu, A. Brăileanu, C. Radovici, M. Ban, J. Madarász and G. Pokol, Proceedings of the 3rd International Conference on Global Research and Education in Intelligent Systems, Inter-Academia 2004, September 6–9, 2004 Budapest, Hungary, Vol. II, p. 251.
16 R. A. Nyquist and R. O. Kagel, ‘Infrared spectra of inorganic compounds’, Ed. Academic Press, New York and London 1963, p. 543.
17 Z. C. Orel, Internet J. Vib. Spec., 3, 4, 6 (1999).